*I.J. Information Technology and Computer Science,* **2026, 5, 138-150**
Published Online on October 8, 2026 by MECS Press (http://www.mecs-press.org/)
DOI: 10.5815/ijitcs.2026.05.09

# Carbon Dioxide Emission Prediction for Trend Analysis using CAViaR Pine Cone Optimization Algorithm Enabled Attention-Based LSTM

**Choudari Lakshmi***
Department of CSE, GITAM Visakhapatnam, India
E-mail: lchoudar@gitam.edu
ORCID iD: https://orcid.org/0000-0002-4971-3787
*Corresponding author

**Srinivasa Rao Konda**
Department of CSE, GITAM Visakhapatnam, India
E-mail: skonda@gitam.edu
ORCID iD: https://orcid.org/0000-0002-1726-5692

Received: March 1, 2026; Revised: May 8, 2026; Accepted: July 23, 2026; Published: October 8, 2026

**Abstract:** Predicting Carbon dioxide ($CO_2$) emissions is essential for guiding environmental policies and climate strategies, yet accurate local-scale prediction remains challenging due to complex spatial and temporal factors. Existing approaches often focus on regional or global models and do not fully exploit high-resolution satellite imagery for local trend analysis. To overcome these limitations, Conditional Pine Cone Optimization enabled Attention-Based Long Short-Term Memory (CPCO_ALSTM) is devised for $CO_2$ Emission prediction for Trend Analysis in Satellite Image. In this approach, satellite images of the query region acquired at different time intervals are used as input. Initially, a Kalman Filter is employed for noise reduction and temporal smoothing during preprocessing. Then, segmentation of satellite image is done using Dense-Res Recurrent Prototypical Network (DRRP-Net), wherein DRRP-Net is developed by combining Dense-Res-Inception Network (DRINet) and Recurrent Prototypical Network (RP-Net). Based on the segmented regions and extracted features, carbon emission estimation is carried out. The estimated $CO_2$ emissions are then validated against ground-truth emission data obtained from a reference database to assess prediction accuracy. For temporal trend analysis, an Attention-Based Long Short-Term Memory (ALSTM) model is utilized to capture long-range dependencies in emission patterns. The ALSTM parameters are optimally tuned using the proposed CPCO algorithm, which combines Pine Cone Optimization (PCO) with Conditional Autoregressive Value at Risk (CAViaR) to enhance convergence stability and prediction robustness. Additionally, CPCO_ALSTM has attained 96.35% of accuracy, 0.087 of normalized MSE, and 0.957 of Jaccard Coefficient.

**Index Terms:** Carbon Dioxide Emission, Trend Analysis, Satellite Image, Long Short-Term Memory, Conditional Autoregressive Value at Risk.

## 1. Introduction

Climate change, which is driven mainly by the rise in greenhouse gases, like $CO_2$, is one of the most urgent global challenges today. Human activities, such as burning fossil fuels, deforestation, industrial processes, agriculture, urbanization, transportation, mining, and waste disposal release large amounts of $CO_2$ into the atmosphere, which is the leading cause of global warming (IPCC, 2021) [1]. This increase in $CO_2$ leads to rising temperatures, environmental damage, more frequent extreme weather events, and serious risks to human health and ecosystems [2]. To address this, global greenhouse gas emissions must be reduced by at least 50% by 2050, with a strong emphasis on cutting $CO_2$ emissions, even as energy demands continue to grow [1]. Essential strategies include adopting renewable energy, improving energy efficiency, and deploying carbon capture technologies [3]. Accurate forecasting and continuous monitoring of emissions support effective policymaking and track progress towards targets [1]. Although natural sources, such as organic decomposition, ocean release, and volcanic activity contribute some $CO_2$, their impact is small compared to anthropogenic emissions [2]. Addressing these challenges is essential for a resilient and sustainable future; moreover,

This work is open access and licensed under the Creative Commons CC BY 4.0 License.

Satellite imagery significantly contributes by offering critical geographical data. Thus, it supports environmental monitoring, disaster management, and informed decision-making in response to climate change and other global environmental issues [4].

Many studies have investigated global $CO_2$ emissions across both developed and developing nations using a variety of statistical methods. These studies often identify a strong connection between rising $CO_2$ levels and increased energy use driven by economic growth and development. Scarcity of long-term data is a key challenge, which is essential for accurate trend analysis over several decades. Short data records and small sample sizes hinder the ability to detect meaningful changes and interpret trends reliably. Furthermore, detailed historical and sector-specific emissions data are limited [2]. Understanding long-term $CO_2$ emission patterns is vital for forecasting economic growth and creating effective strategies to reduce emissions while safeguarding public health and the environment [5] [3]. While several forecasting techniques exist, such as econometric models, input-output models, and surveys, trend analysis is widely favored for its simplicity and dependence on available data [3]. Moreover, trend analysis was used to project energy-related $CO_2$ emissions for the top 25 countries and global total between 1971 and 2007. Emission data from the International Energy Agency were analyzed using least squares regression to ensure statistical reliability [3]. Hence, it provides dependable projections to aid in policy formulation and environmental planning.

The main intention is to develop a novel approach for predicting $CO_2$ emissions on Trend Analysis in Satellite Image Time Series using CPCO_ALSTM. For trend analysis, the satellite image of Query region is considered for each interval as input, and a Kalman filter accomplishes preprocessing. Then, segmentation of satellite image is done using DRRP-Net, wherein DRRP-Net is developed by merging DRINet and RP-Net. Then, estimation of carbon emissions is performed. Moreover, estimated carbon emission amount is compared with original $CO_2$ emission from database for accuracy. Here, Trend Analysis is performed using ALSTM, which is trained using CPCO. Here, the integration of PCO and CAViaR develops CPCO.

Major contribution of this research is mentioned below.

- Devised CPCO_ALSTM for $CO_2$ emission prediction on Trend Analysis: An innovative model called CPCO_ALSTM is devised to predict $CO_2$ Emission. In this work, prediction of $CO_2$ emissions using trend analysis is performed using ALSTM. Here, ALSTM is trained using CPCO, the integration of PCO and CAViaR develops CPCO.

The layout of the following sections is as follows: A review of the literature on existing methods for $CO_2$ emission prediction is provided in Section 2; Methodology and architecture of the devised method are detailed in Section 3; Evaluation outcomes and ablation study are detailed in Section 4; Additionally, in Section 5, conclusion and future work are summarized.

## 2. Motivation

Development of a new model for predicting $CO_2$ emissions using trend analysis is driven by the demand for precise, long-term forecasts that can inform effective climate policies. Many current models are constrained by limited data availability or require complex assumptions. By using a straightforward, data-focused trend analysis, more reliable predictions can be made even with minimal data. This method seeks to improve policy decisions related to emission reduction and environmental management.

### *2.1. Literature Review*

J. D. L. Brazidec, *et al.* [6] developed a $CO_2$ emission prediction method named Convolutional neural networks (CNN). This method effectively modified $CO_2$ plumes from power, although it struggled to account for outliers, such as plants with exceptionally high emissions. A. Danjou, *et al.* [7] introduced a method for predicting $CO_2$ emissions namely, Decision tree learning. The model accurately segmented the images for estimation purposes; However, it failed to collect more spatial variability of $CO_2$ emissions. B. F. Andrade, *et al.* [8] presented a Cross-sectional mass balance approach for predicting $CO_2$ emission. It eliminated the comparison between bottom-up and top-down evaluations but overlooked local-scale emissions, leading to inaccuracies in the overall emission estimation. S. N. Wren, *et al.* [9] developed FNO-DenseNet based on Fourier neural operator (FNO) for carbon emission prediction. It was easily scalable to larger regions, but it lacked the ability to predict Soil Organic Carbon (SOC) at fine resolutions.

### *2.2. Challenges*

Main challenges experienced by traditional methods on $CO_2$ Emission prediction are mentioned as follows.

- The CNN model presented in [6] effectively addressed missing data due to cloud cover. Still, it did not incorporate the crucial classification of high-frequency regions, such as urban areas.
- In [7], the developed model improved insights into urban $CO_2$ emissions; however, it omitted the use of satellite image-based emission estimation.
- Although the model in [8] showed promise for monitoring $CO_2$ emissions from specific power plants, the limited

spatial resolution of satellite imagery restricted its ability to capture detailed local emission patterns.

- Reliable and accurate $CO_2$ emission data is essential for effective prediction, yet data availability and quality often pose challenges, particularly in developing regions with limited monitoring infrastructure.

## 3. Proposed Conditional Pine Cone Optimization enabled Attention-Based Long Short-Term Memory for $CO_2$ Emission prediction using Trend Analysis

Analyzing satellite images has become an essential method for tracking environmental changes, urban growth, deforestation, and agricultural developments over time. While traditional models have been commonly applied for trend detection, they often face challenges due to the complex, nonlinear, and noisy nature of satellite data. These conventional techniques usually rely on assumptions of stationarity, struggle with missing data and seasonal effects, and have limited ability to detect subtle or rapid changes in land conditions. Hence, innovative model is developed for $CO_2$ Emission prediction on Trend Analysis in Satellite Image Time Series using CPCO_ALSTM. In this work, $CO_2$ is not directly detected from satellite images. Instead, a specific geographic area is cropped from the satellite image, and the corresponding $CO_2$ emission values for that region are obtained from the dataset. For trend analysis, at every time interval , and , the satellite image of Query region is considered as an input and is preprocessed by Kalman filter. After that, segmentation of satellite image is done using DRRP-Net, wherein DRRP-Net is developed by merging DRINet and RP-Net. The segmentation is done into major land-cover classes, such as buildings, roads, vegetation, water bodies, and open land. Then, carbon emissions estimation is performed. Moreover, carbon emissions are estimated and compared with original $CO_2$ from the database for accuracy. Here, Trend Analysis is performed using ALSTM, which is trained using CPCO. Here, the integration of PCO and CAViaR develops CPCO. Additionally, schematic structure of developed CPCO_ALSTM to predict $CO_2$ emission on Trend Analysis is illustrated in Fig. 1

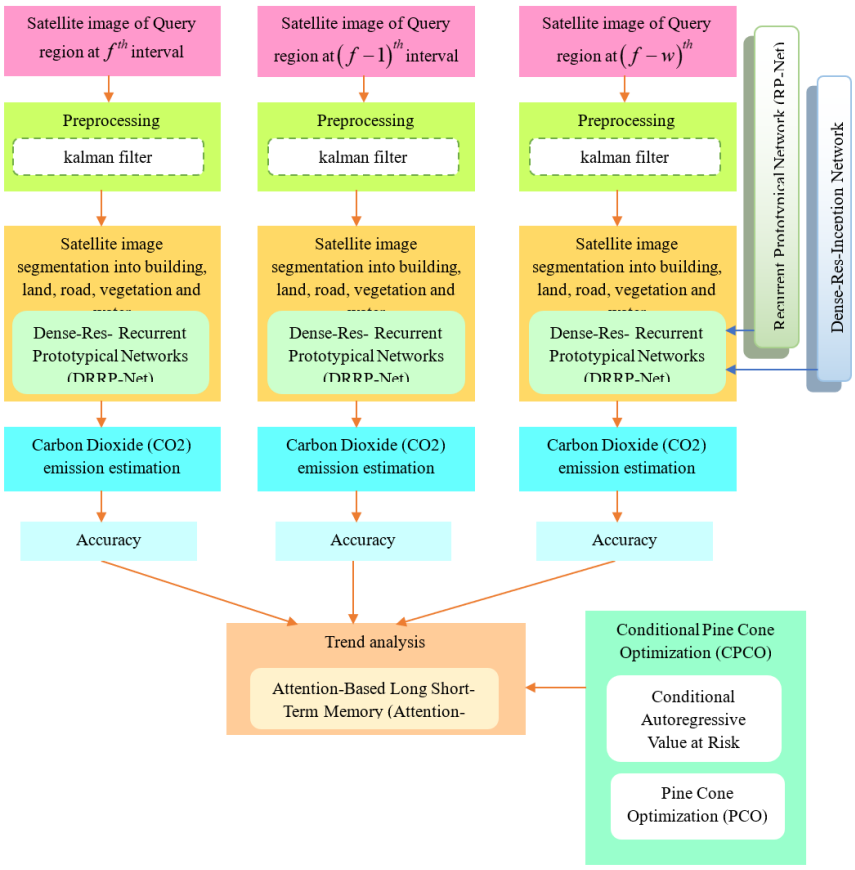



Fig. 1. Schematic structure of developed CPCO_ALSTM for $CO_2$ emission prediction on trend analysis

### *3.1. Satellite image Acquisition from Bhoonidhi and Climate Watch dataset*

The Bhoonidhi dataset [10] is a comprehensive collection of high-resolution satellite imagery used for land use and land cover mapping in India. Here, at the dataset , the images at the interval are given as,

$$H = \left\{ H_1^f, H_2^f, ..., H_q^f, ..., H_\eta^f \right\} \tag{1}$$

where, the total images in the dataset $H$ at $f^{th}$ interval is indicated as $H_{\eta}^{f}$, randomly selected $q^{th}$ sample from dataset is implied as $H_{q}^{f}$. Similarly, at time interval $f+1$ and $f-w$ the randomly chosen image is considered as $H_{q}^{f+1}$ and $H_{q}^{f-w}$ respectively. Additionally, the Climate Watch dataset [11] offers extensive worldwide information on greenhouse gas emissions, climate policies, and environmental metrics to aid in climate research and decision-making, and at $f^{th}$ interval, it is expressed as,

$$P=\left\{P_{1}^{f},P_{2}^{f},...,P_{q}^{f},...,P_{\eta}^{f}\right\} \tag{2}$$

Here, Climate Watch dataset is signified as $P$, total images in the dataset is represented as $P_{\eta}^{f}$, and the $q^{th}$ image that is chosen randomly from dataset is implied as $P_{q}^{f}$. Likewise, it is processed for every time interval. In this work, the sample at time $H_{\eta}^{f}$ is selected for further analysis.

*3.2. Image Preprocessing at Every Time Interval Using Kalman Filter*

At every time interval, images undergo preprocessing to improve their quality and make them suitable for further analysis. Here, image $H_{q}^{f}$ is preprocessed using Kalman filter as it effectively reduces noise and provides optimal estimates in dynamic and time-varying images.

*A. Kalman Filter*

The Kalman filter [12] is used for pre-processing. The cropped satellite image region is first converted into a structured representation, and the Kalman filter is used as a recursive noise-reduction estimator to smooth measurement inconsistencies across spectral bands and acquisition noise. It is calculated using below expression,

$$A_{h}^{*}=W_{h}^{z}I_{h}^{\Upsilon}\left(I_{h}W_{h}^{z}I_{h}^{\Upsilon}+O_{h}\right)^{-1} \tag{3}$$

$$u_{h}^{s}=u_{h}^{z}+A_{h}^{*}\left(v_{h}-I_{h}u_{h}^{z}\right) \tag{4}$$

$$W_{h}^{s}=\left(1-A_{h}^{*}I_{h}\right)W_{h}^{z} \tag{5}$$

where, Kalman gain is indicated as $A_{h}^{*}$, forecast error covariance matrix is signified as $W^{z}$, observation error covariance matrix is implied as $O_{h}$, analysis error covariance matrix is indicated as $W_{h}^{s}$, observation operator is denoted as $I_{h}^{\Upsilon}$, prediction error covariance matrix is implied as $W_{h}^{z}$, predicted value is represented as $u_{h}^{z}$, analysis value is implied as $u_{h}^{a}$, and observation is signified as $v$. Then, the obtained preprocessed image at $f^{th}$ interval is indicated as $R_{q}^{f}$, similarly, $R_{q}^{f+1}$ at $\left(f+1\right)^{th}$ interval, and $R_{q}^{f-w}$ at $\left(f-w\right)^{th}$ interval.

*3.3. Satellite Image Segmentation at Every Time Using DRRP-Net*

At each time interval, satellite images are segmented to identify and separate distinct regions, enabling precise analysis of land surface variations. Here, the preprocessed image $R_{q}^{f}$ is allowed for segmentation of satellite image using DRRP-Net, whereas DRRP-Net is developed by integrating DRINet with RP-Net. The prototype-learning mechanism of RP-Net is adopted to improve class representation and boundary discrimination in heterogeneous land-cover regions (e.g., buildings, roads, vegetation, and water). The DRINet is employed to enhance multi-scale feature extraction, which is important because satellite imagery contains objects of highly varying spatial scales. The residual and dense connections improve gradient flow and feature reuse, reducing information loss. Additionally, network structure of DRRP-Net is illustrated in Fig. 2.

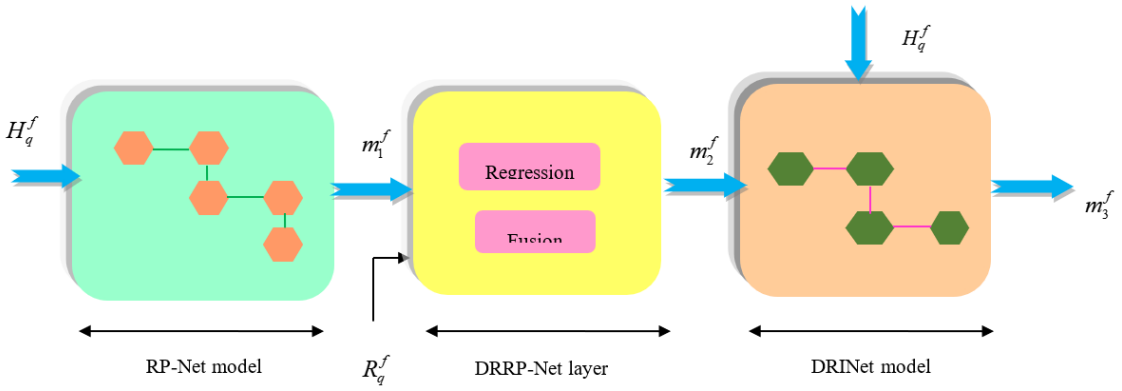



Fig. 2. Network structure of DRRP-Net

In RP-Net [13] model, the input image $H_q^f$ is utilized as an input. Additionally, the outcome $m_1^f$ is expressed as,

$$m_1{}^{f(\alpha,\beta)} = \arg_{\chi} \max m_{soft}^{(\alpha,\beta,\chi)} \tag{6}$$

where, spatial position of binary mask is indicated as $(\alpha,\beta,\chi)$, soft max is signified as $m_{soft}$. Then, the output of RP-Net model $m_1^f$ along with preprocessed image $R_q^f$ is fed into DRRP-Net layer, and is formulated below.

$$m_2 = 2\sum_{\mu=1}^{(\phi-\vartheta)}\sum_{\varsigma=1}^{\nu}\sum_{\varepsilon=1}^{\vartheta} R_{q(\mu,\varsigma,\varepsilon)} * \Psi_{(\mu,\varsigma,\varepsilon)} - \arg_{\chi} \max m_{soft}^{(\alpha,\beta,\chi)} \tag{7}$$

where, the preprocessed image's size is indicated as $\vartheta$ and $\nu$, weight is implied as $\Psi$, and $R_q^f$ implies the preprocessed image. In the DRINet Model [14], the resultant of DRRP-Net layer $m_2^f$ with input image $H_q^f$ is proceeded, and its expression is evaluated below,

$$m_3^f = \mathbb{Z}\left(2\sum_{\mu=1}^{(\phi-\vartheta)}\sum_{\varsigma=1}^{\nu}\sum_{\varepsilon=1}^{\vartheta} R_{q(\mu,\varsigma,\varepsilon)} * \Psi_{(\mu,\varsigma,\varepsilon)} - \arg_{\chi} \max m_{soft}^{(\alpha,\beta,\chi)}\right) \tag{8}$$

Thus, the resultant segmented image obtained from DRRP-Net at $f^{th}$ interval is indicated as $m_3^f$. Likewise, the outcome attained at $(f+1)^{th}$ interval is $m_3^{f+1}$, and at $(f-w)^{th}$ interval is $m_3^{f-w}$.

### *3.4. Carbon Estimation at Regular Time Intervals for $CO_2$ Emission Analysis*

Carbon estimation [15] at regular time intervals enables accurate analysis and monitoring of $CO_2$ emissions over time. Carbon emission estimation calculates the greenhouse gases produced by transport, energy consumption, and industrial processes. This process supports environmental monitoring and sustainable decision-making.

$$C = \sum_{d=1}^{b} N_d * \Pi_d \left(\frac{JCO_2}{JC}\right) \tag{9}$$

Here, $CO_2$ emissions derived from classified land areas are indicated as $C$, the average values of different land use types are represented as $N_d$ and $\Pi_d$. This involves applying specific carbon emission coefficients and accounting for the number of occurrences of each land use category, where, $\frac{JCO_2}{JC} = \frac{44}{12} = 3.667$. The result generated from this stage reflects the overall carbon balance. Then, the obtained carbon estimated outcome is $P_q^f$ at $f^{th}$ interval, similarly, $P_q^{f+1}$ at $(f+1)^{th}$ interval, and $P_q^{f-w}$ at $(f-w)^{th}$ interval.

### *3.5. Trend Analysis*

Trend analysis of carbon emission estimation involves examining emission data over time to identify consistent patterns or changes in greenhouse gas outputs. In this work, trend analysis is carried out using an ALSTM model, which is trained with the CPCO. Furthermore, CPCO is a hybrid approach that integrates CAViaR with PCO to enhance training performance.

#### *A. ALSTM*

The ALSTM model [16] employs a neural network to predict the nonlinear seismic behavior of bridges by incorporating a temporal attention mechanism into a traditional encoder-decoder framework. In this ALSTM model, the $CO_2$ emissions estimated outcome $P_q^f$ is fed as an input. This attention mechanism enables the network to concentrate on the most important features within time-series data. The architecture comprises six main components: an input, encoder, attention, decoder, and output phase. Encoder as well as decoder contains LSTM layers followed by two fully connected layers, which are utilized by attention block with activation function. ReLU activation and dropout layers (rate of 0.2) are applied to prevent overfitting and vanishing gradients. The ALSTM model's structure is illustrated in Fig. 3.

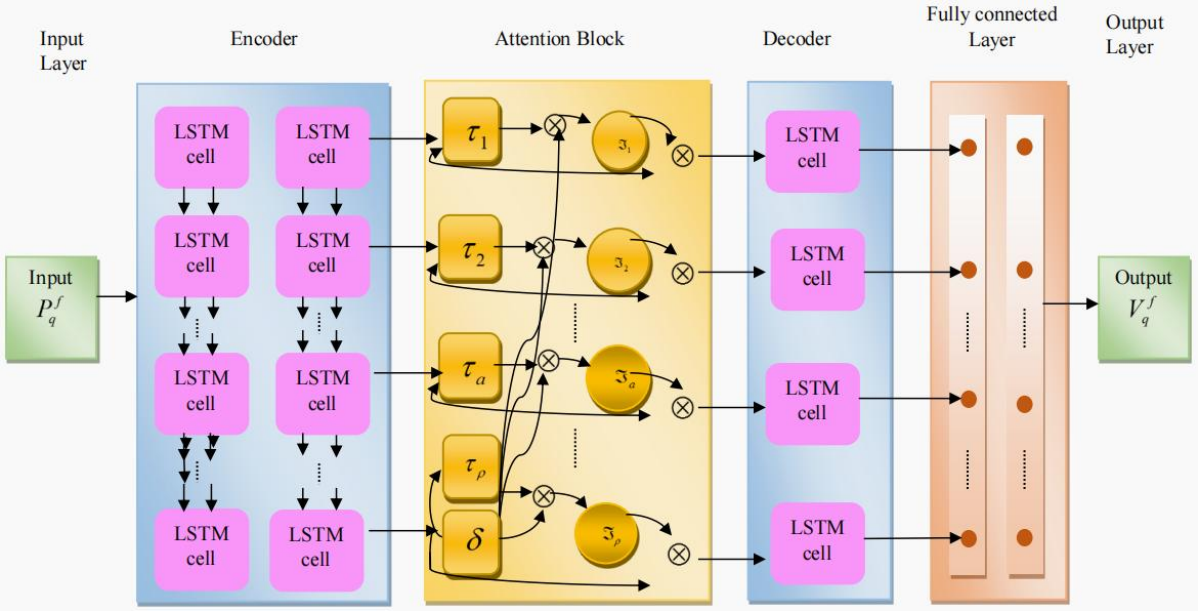



Fig. 3. Structure of ALSTM

Moreover, the output attained from ALSTM network is indicated as $V_q^f$ at $f^{th}$ interval, likewise, $V_q^{f+1}$ at $\left(f+1\right)^{th}$ interval, and $V_q^{f-w}$ at $\left(f-w\right)^{th}$ interval.

#### *B. Tuning of ALSTM using CPCO*

Tuning is performed to train the network for increased accuracy and reliability of $CO_2$ emission estimation. Here, ALSTM is trained using CPCO, which is the combination of CAViaR with PCOA [17]. PCOA is based on the behavior of pine cones to solve complex optimization issues. The conditional autoregressive structure of CAViaR is adapted as a dynamic updating mechanism to control the optimization search behavior under varying error distributions during hyperparameter tuning. Specifically, it is used to model conditional variations in the loss function, thereby improving stability and preventing extreme parameter fluctuations during optimization.

- ***Solution Encoding:*** It is used to represent a potential solution by defining its position within a specified search space. Additionally, it is expressed as $so\ln = \left[1 \times \mathbb{R}\right]$, where hyperparameter of ALSTM is indicated as.
- ***Evaluation of fitness:*** It is the discrepancy between predicted value and actual target value to determine optimal result. The calculation is carried out as follows,

$$fitness = \frac{1}{\eta}\sum_{q=1}^{n}\left(V_q^{f*} - V_q^f\right)^2 \tag{10}$$

where, $\eta$ indicates entire images in database, targeted outcome is denoted as $V_q^{f*}$ and actual outcome is indicated as $V_q^f$. Additionally, CPCO method's algorithmic steps are as follows.

*Step 1. Population Initialization*

During initialization, pine trees and cones are used to divide the problem space into segments. In this space, trees are located at the middle of each segment and cones are initialized around them within defined boundaries

*Step 2: Exploitation Phase*

In this phase, the search space is partitioned into super-cubes and this process imitates the behavior of cones dispersing as they fall under the influence of gravity.

*Step 3: Exploration Phase*

To mimic the pollination of pine tree, PCOA uses two distinct mechanisms modeling agents from male cones reaching female cones within or between trees, represented by the following formulation.

$$yB_{i,j}^{new} = yB_{i,j} + 0.5 \times \Re_{\varepsilon_1} \times \left( trbst_i - tB_{\varepsilon_1,j} \right) + 0.5 \times \Re_{\varepsilon_3} \times \left( trbst_i - yB_{\varepsilon_3,j} \right) \tag{11}$$

where, position of cone is indicated as $yB$, index of cone is represented as $i$, best position of tree is indicated as $trbst$, index of tree is implied as $j$, and chance of successful pollination is indicated as.

By CAViaR,

$$yB_{i,j}^{n} = \ell_0 + \sum_{r=1}^{p} \ell_r yB_{i,j}^{n-r} + \sum_{c=1}^{t} \ell_c \rho \left( yB_{i,j}^{n-t} \right) \tag{12}$$

Let $p = t = 2$,

$$yB_{i,j}^{n} = \ell_0 + \ell_1 yB_{i,j}^{n-1} + \ell_2 yB_{i,j}^{n-2} + \ell_1 \rho \left( yB_{i,j}^{n-1} \right) + \ell_2 \rho \left( yB_{i,j}^{n-2} \right) \tag{13}$$

Substituting Eq. (13) in Eq. (11),

$$\begin{aligned} yB_{i,j}^{new} = & \left( \ell_0 + \ell_1 yB_{i,j}^{n-1} + \ell_2 yB_{i,j}^{n-2} + \ell_1 \rho \left( yB_{i,j}^{n-1} \right) + \ell_2 \rho \left( yB_{i,j}^{n-2} \right) \right) \\ & + 0.5 \times \Re_{\varepsilon_1} \times \left( trbst_i - tB_{\varepsilon_1,j} \right) + 0.5 \times \Re_{\varepsilon_3} \times \left( trbst_i - yB_{\varepsilon_3,j} \right) \end{aligned} \tag{14}$$

where, $\ell$ is a constant, position of cone is indicated as $yB$, index of cone is represented as $i$, best position of tree is indicated as $trbst$, index of tree is implied as $j$, and successful pollination's chance is implied as.

*Step 4: Animals dispersing pine cones*

Inspired by the natural behavior of animals dispersing pine cones, the algorithm employs four operators. One of these involves relocation of a cone by a squirrel from a random location to an optimal position, which is guided by quadratic programming to enhance solution quality.

*Step 5: Assigning cones to every tree*

Each tree adjusts the positions of nearby cones to realistically mimic the natural pattern of falling. Over successive generations, this process attracts nearby cones and allows well-positioned trees to gather more cones

*Step 6: Fitness Re-calculation*

CPCO algorithm continues to iterate until optimal solution is achieved by Eq. (10).

*Step 7: Termination*

In termination step, CPCO algorithm concludes once optimal solution has been successfully obtained.

*3.6. Accuracy Calculation*

To evaluate the accuracy of CO2 emission estimates, the predicted values are compared against actual data obtained from a reliable database. This evaluation is performed at regular time intervals, allowing for continuous monitoring and

prediction of CO2 emissions over time.

## 4. Result and Discussion

The devised CPCO_ALSTM for predicting $CO_2$ emission for Trend Analysis is evaluated, and its dataset description is mentioned in this part.

*4.1. Experimental Setup*

The CPCO_ALSTM model for $CO_2$ emission prediction and trend analysis is implemented using the Python tool.

*4.2. Dataset Description*

In this study, the satellite imagery is obtained from the Bhoonidhi geo-portal, which is maintained by the Indian Space Research Organization (ISRO) [10]. Specifically, Level-2 products from the Resourcesat-2 mission are used, including LISS-3 and LISS-4 (MX70) sensors. The Resourcesat-2 LISS-3 (L2) data provide a spatial resolution of 23.5 meters and include four spectral bands: Green (0.52–0.59 μm), Red (0.62–0.68 μm), Near Infrared (0.77–0.86 μm), and Shortwave Infrared (1.55–1.70 μm). The Resourcesat-2 LISS-4 (MX70, L2) data offer a higher spatial resolution of 5.8 meters and include three spectral bands: Green (0.52–0.59 μm), Red (0.62–0.68 μm), and Near Infrared (0.77–0.86 μm) [11]. The combination of moderate (23.5 m) and high (5.8 m) spatial resolution imagery enables detailed land-cover segmentation of buildings, roads, vegetation, water bodies, and open land areas. The inclusion of Near Infrared and Shortwave Infrared bands enhances vegetation discrimination and surface material characterization, which are essential for extracting emission-related spatial proxies used in indirect $CO_2$ emission estimation.

*4.3. Evaluation Metrics*

To analyze the efficiency of devised CPCO_ALSTM for $CO_2$ Emission prediction, metrics like normalized MSE, accuracy, and Jaccard coefficient are utilized.

*A. Normalized MSE*

Normalized MSE is used to measure the difference between the predicted and actual continuous $CO_2$ emission values after normalization.

*B. Accuracy*

Accuracy is used to evaluate the correctness of emission range prediction after dividing the continuous $CO_2$ values into 10 emission bins. It measures the proportion of samples for which the predicted emission range matches the actual emission range.

*C. Jaccard Coefficient*

The Jaccard Coefficient is used to measure the similarity between the predicted and actual emission classes after dividing the $CO_2$ values into 10 bins emission ranges. It is calculated as the ratio of correctly predicted samples to the total unique samples present in either the predicted or actual class.

*4.4. Comparative Methods*

CNN [6], Global adaptive-mesh model [7], Cross-sectional flux method [8], FNO-DenseNet [9], UNet-FCNN, and DRRP-Net are the comparative methods that are used to analyze the performance of CPCO_ALSTM.

*4.5. Comparative Assessment*

The efficiency of the developed CPCO_ALSTM is evaluated using various metrics by varying delay and training data.

*A. Assessment based on Delay*

Evaluation of CPCO_ALSTM with comparative techniques, like CNN, Global adaptive-mesh model, Cross-sectional flux method, FNO-DenseNet, UNet-FCNN, and DRRP-Net, by changing delay from 5 to 25 years, is illustrated in Fig. 4. In Fig. 4 a), Analysis of CPCO_ALSTM with respect to accuracy is illustrated. For delay of 25 years, accuracy of CPCO_ALSTM is 96.16%, while other traditional approaches have achieved an accuracy of 84.13%, 87.16%, 88.65%, 90.74%, 92.88%, and 94.06%. Fig. 4 b) illustrates the analysis of CPCO_ALSTM in normalized MSE. For delay = 25 years, conventional methods have reached normalized MSE of 0.431, 0.386, 0.326, 0.268, 0.202, and 0.115. Moreover, CPCO_ALSTM has achieved a low normalized MSE rate of 0.095. In addition to this, Fig. 4 c) shows the evaluation of CPCO_ALSTM in terms of Jaccard Coefficient. Here, CPCO_ALSTM has reached 0.955 Jaccard coefficient, whereas, traditional approaches have attained 0.854, 0.871, 0.883, 0.891, 0.913, and 0.932 of Jaccard Coefficient value.

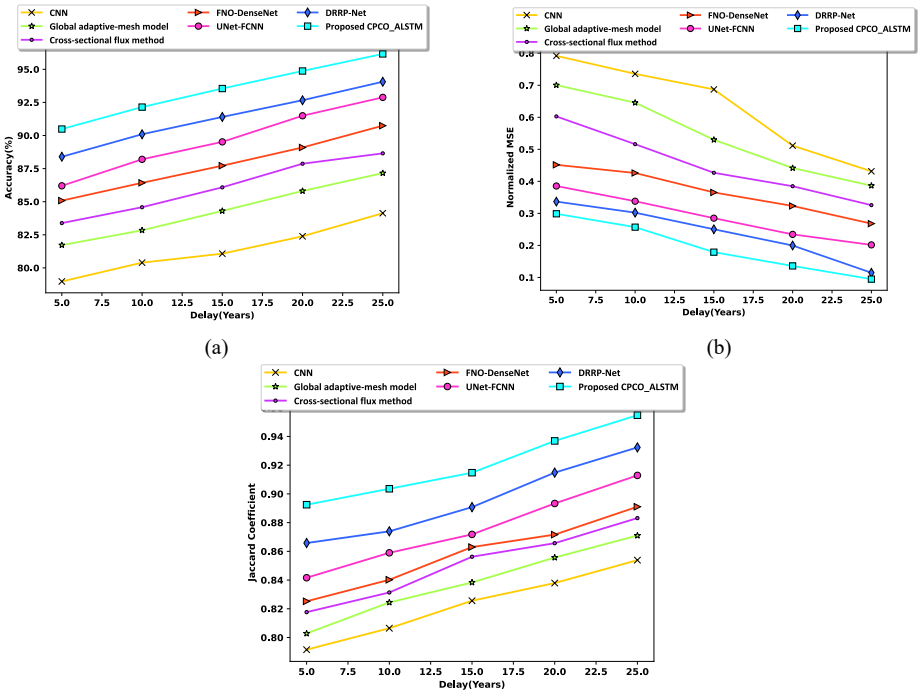



Fig. 4. Comparative evaluation of CPCO_ALSTM based on delay, a) Accuracy, b) Normalized MSE, c) Jaccard Coefficient

*B. Assessment based on Training Data*

Fig. 5 shows assessment of CPCO_ALSTM with traditional methods, such as CNN, Global adaptive-mesh model, Cross-sectional flux method, FNO-DenseNet, UNet-FCNN, and DRRP-Net, by changing delay. Moreover, 90% training data is considered in this assessment. Fig. 5 a) portrays the analysis of CPCO_ALSTM with respect to accuracy. The accuracy attained by CPCO_ALSTM is 96.35%, while baseline methods have achieved an accuracy of 85.11%, 87.37%, 88.78%, 90.93%, 92.94%, and 94.35%, respectively. Assessment of CPCO_ALSTM for normalized MSE is displayed in Fig. 5 b). Conventional methods have reached normalized MSE of 0.331, 0.301, 0.275, 0.221, 0.187, and 0.104. Additionally, CPCO_ALSTM has achieved a low normalized MSE rate of 0.087. Fig. 5 c) illustrates the evaluation of CPCO_ALSTM in accordance with Jaccard Coefficient. Here, CPCO_ALSTM has reached 0.957 Jaccard coefficient, however, traditional approaches have attained 0.855, 0.866, 0.874, 0.897, 0.908, and 0.936 of Jaccard Coefficient value.

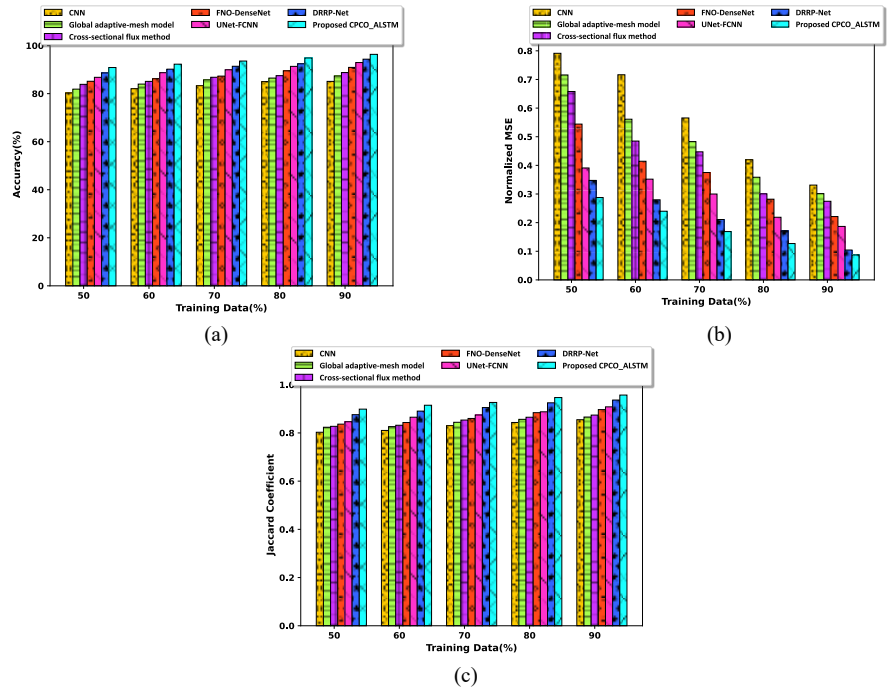



Fig. 5. Comparative evaluation of CPCO_ALSTM based on training data, a) Accuracy, b) Normalized MSE, c) Jaccard Coefficient

### *4.6. Algorithmic Assessment*

The algorithmic performance of CPCO_ALSTM is compared with Adam_ALSTM [18], RMSProp_ALSTM [19], and Bayesian Optimization_ALSTM [20] and the results are provided in Fig. 6. The results obtained on population size 50 are discussed in this section. Fig. 6 a) portrays the analysis with respect to accuracy. The accuracy attained by CPCO_ALSTM is 95.64%, while Adam_ALSTM, RMSProp_ALSTM, and Bayesian Optimization_ALSTM have achieved an accuracy of 92.74%, 93.63%, and 94.32%. Assessment for normalized MSE is displayed in Fig. 6 b). The Adam_ALSTM, RMSProp_ALSTM, and Bayesian Optimization have reached normalized MSE of 0.192, 0.150, and 0.112 and the CPCO_ALSTM has achieved a low normalized MSE rate of 0.090. Fig. 6 c) illustrates the evaluation in accordance with Jaccard Coefficient. Here, CPCO_ALSTM has reached 0.958 Jaccard coefficient, however, Adam_ALSTM, RMSProp_ALSTM, and Bayesian Optimization_ALSTM have attained 0.914, 0.929, and 0.940 of Jaccard Coefficient value.

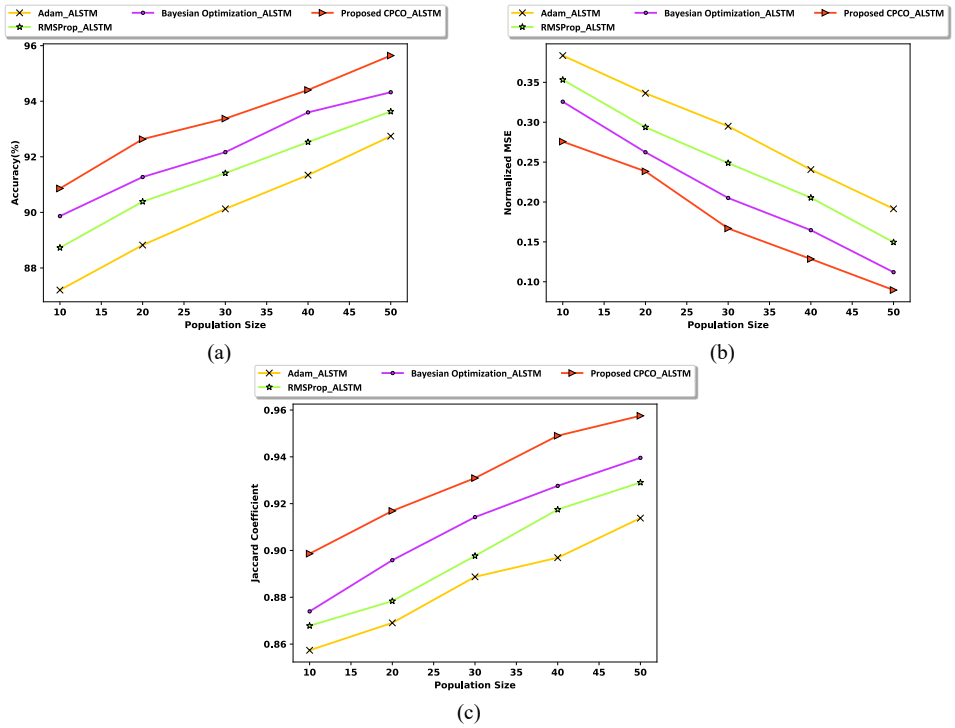



Fig. 7. Algorithmic evaluation of CPCO_ALSTM based on population size, a) Accuracy, b) Normalized MSE, c) Jaccard Coefficient

Table 1. Comparative discussion of CPCO_ALSTM for $CO_2$ emission estimation

| Variation | Metrics | CNN | Global adaptive-mesh model | Cross-sectional flux method | FNO-Dense Net | UNet-FCNN | DRRP-Net | Proposed CPCO_ALSTM |
|---|---|---|---|---|---|---|---|---|
| Delay= 100s | Accuracy (%) | 84.13 | 87.16 | 88.65 | 90.74 | 92.88 | 94.06 | 96.16 |
| | Normalized MSE | 0.431 | 0.386 | 0.326 | 0.268 | 0.202 | 0.115 | 0.095 |
| | Jaccard Coefficient | 0.854 | 0.871 | 0.883 | 0.891 | 0.913 | 0.932 | 0.955 |
| Training Data 90% | Accuracy (%) | 85.11 | 87.37 | 88.78 | 90.93 | 92.94 | 94.35 | **96.35** |
| | Normalized MSE | 0.331 | 0.301 | 0.275 | 0.221 | 0.187 | 0.104 | **0.087** |
| | Jaccard Coefficient | 0.855 | 0.866 | 0.874 | 0.897 | 0.908 | 0.936 | **0.957** |

### *4.7. Comparative Discussion*

Table 1 demonstrates CPCO_ALSTM method's comparative discussion for $CO_2$ Emission estimation in which efficiency of CPCO_ALSTM is compared with competitive methods, like CNN, Global adaptive-mesh model, Cross-sectional flux method, FNO-DenseNet, UNet-FCNN, and DRRP-N. It is performed by varying delay and training data. Here, conventional approaches have attained accuracy of 89.42%, 90.91%, 92.41%, and 94.27%, whereas CPCO_ALSTM has attained 96.35% of accuracy. Additionally, 0.331, 0.301, 0.275, 0.221, 0.187, and 0.104 are error values attained by traditional approaches. Moreover, CPCO_ALSTM has reached a low normalized MSE rate of 0.087. Additionally, CPCO_ALSTM has achieved a Jaccard Coefficient value of 0.957. However, other techniques have reached

Jaccard Coefficient values of 0.855, 0.866, 0.874, 0.897, 0.908, and 0.936. This demonstrates that CPCO_ALSTM for $CO_2$ emission estimation method has strong reliability, precision, and effectiveness in identifying emission patterns.

## 5. Conclusions

Estimating $CO_2$ emissions is crucial for forecasting pollution levels and supporting climate-related strategies and decisions. Conventional methods often struggle with poor prediction accuracy, lack flexibility, and are ineffective in managing rapidly changing emission patterns. Here, CPCO_ALSTM is designed to predict $CO_2$ emission on Trend Analysis in Satellite Image. At every time interval, the input image is acquired and is preprocessed using Kalman filter. Thereafter, segmentation of satellite image is done using DRRP-Net, wherein DRRP-Net is developed by merging DRINet with RP-Net. Then, carbon emissions estimation is achieved. Moreover, the estimated amount of carbon emissions is compared with the actual $CO_2$ emissions from the database to assess accuracy. Here, Trend Analysis is performed using ALSTM, which is trained using CPCO. Here, the integration of PCO and CAViaR develops CPCO. Additionally, CPCO_ALSTM has attained 96.35% of accuracy, 0.087 of normalized MSE, and 0.957 of Jaccard Coefficient. Future work lies in enhancing model accuracy, scalability, and adaptability by integrating advanced optimization to better capture dynamic and complex emission behaviors.

## All the Declarations and Statements

### Author Contributions Statement

Choudari Lakshmi: Conceptualization, Methodology, Algorithm Development, Software Implementation, Data Curation, and Writing – Original Draft Preparation.
Srinivasa Rao Konda: Supervision, Validation, Review & Editing, and Guidance of the research work.

All authors have read and agreed to the published version of the manuscript.

### Conflict of Interest Statement

The authors declare no conflicts of interest.

### Funding Declaration

This research received no external funding.

### Data Availability Statement

The dataset used in this study is obtained from publicly available datasets, namely the Bhoonidhi geo-portal maintained by ISRO and the Climate Watch dataset. These datasets are accessible for research purposes.

### Ethical Declarations

None

### Acknowledgments

We would like to thank GITAM (Deemed to be University), Visakhapatnam, for providing the necessary support and facilities to carry out this research work. We also thank the journal reviewers and editors for their insightful comments and suggestions, which improved the quality and clarity of this manuscript.

### Declaration of Generative AI in Scholarity Writing

The authors declare that no generative AI or AI-assisted technologies were used in the preparation of this manuscript. All content, including text, figures, and analysis, were produced directly by the authors.

### Abbreviations

The following abbreviations are used in this manuscript:

$CO_2$ - Carbon Dioxide
CPCO - Conditional Pine Cone Optimization
ALSTM - Attention-Based Long Short-Term Memory
CPCO_ALSTM - Conditional Pine Cone Optimization enabled Attention-Based Long Short-Term Memory
DRRP-Net - Dense-Res Recurrent Prototypical Network
DRINet - Dense-Res-Inception Network
RP-Net - Recurrent Prototypical Network
PCO - Pine Cone Optimization

CAViaR - Conditional Autoregressive Value at Risk
CNN - Convolutional Neural Network
FNO - Fourier Neural Operator
MSE - Mean Squared Error

## Appendix

None.

## References


[1] P. Zhou and M. Wang, "Carbon dioxide emissions allocation: A review," Ecological economics, vol. 125, pp. 47-59, 2016.
[2] "Sources and sectoral trend analysis of CO2 emissions data in Nigeria using a modified Mann-Kendall and change point detection approaches.," Energies, vol. 15, no. 3, p. 766, 2022.
[3] A. C. Kone and T. Buke, "Forecasting of CO2 emissions from fuel combustion using trend analysis.," Renewable and Sustainable Energy Reviews, vol. 14, no. 9, pp. 2906-2915, 2010.
[4] C. Lakshmi and S. R. Konda, "DRRP-Net: Dense-Res-Recurrent Prototypical Networks for carbon emission prediction using satellite image time series," Neurocomputing, vol. 639, p. 130216, 2025.
[5] "Energy, environment and sustainable development," Renewable and sustainable energy reviews, vol. 12, no. 9, pp. 2265-2300, 2008.
[6] J. D. L. Brazidec, P. Vanderbecken, A. Farchi, G. Broquet, G. Kuhlmann and M. Bocquet, "Deep learning applied to CO 2 power plant emissions quantification using simulated satellite images," Geoscientific Model Development Discussions, pp. 1-30, 2023.
[7] A. Danjou, G. Broquet, A. Schuh, F.-M. Bréon and T. Lauvaux, "Optimal selection of satellite XCO2 images over cities for urban CO2 emission monitoring using a global adaptive-mesh model," Atmospheric Measurement Techniques Discussions, pp. 1-33, 2023.
[8] B. F. Andrade, M. Buchwitz, M. Reuter, H. Bovensmann, A. Richter, H. Boesch and P. J. Burrows, "A method for estimating localized CO 2 emissions from co-located satellite XCO 2 and NO 2 images," Atmospheric Measurement Techniques, vol. 17, no. 3, pp. 145-1173, 2024.
[9] S. N. Wren, C. A. McLinden, D. Griffin, S.-M. Li, S. G. Cober, A. Darlington, K. Hayden, C. Mihele, R. L. Mittermeier, M. J. Wheeler, M. Wolde and L. Liggio, "Aircraft and satellite observations reveal historical gap between top–down and bottom–up CO2 emissions from Canadian oil sands," PNAS nexus, vol. 2, no. 5, p. pgad140, 2023.
[10] "Bhoonidhi Dataset," [Online]. Available: https://bhoonidhi.nrsc.gov.in/bhoonidhi/index.html. [Accessed September 2025].
[11] "Climate watch dataset," [Online]. Available: climatewatchdata.org/ghgemissions?end_year=2018&gases=all-ghg%2Cco2&start_year=1990. [Accessed September 2025].
[12] B. Wang, Z. Sun, J. Zeng and R. Liu, "Kalman filter and its application in data assimilation," Atmosphere, vol. 14, no. 8, p. 1319, 2023.
[13] H. Tang, X. Liu, S. Sun, X. Yan and X. Xie, "Recurrent mask refinement for few-shot medical image segmentation," in Proceedings of the IEEE/CVF international conference on computer vision, 2021.
[14] L. Chen, P. Bentley, K. Mori, M. Fujiwara and D. Rueckert, "DRINet for medical image segmentation," EEE transactions on medical imaging, vol. 37, no. 11, pp. 2453-2462, 2018.
[15] M. A. Fattah, S. R. Morshed and S. Y. Morshed, "Multi-layer perceptron-Markov chain-based artificial neural network for modelling future land-specific carbon emission pattern and its influences on surface temperature," SN Applied Sciences, vol. 3, no. 3, p. 359, 2021.
[16] Y. Liao, R. Lin and G. Wu, "Attention-based LSTM (AttLSTM) neural network for seismic response modeling of bridges," Computers & Structures, vol. 275, p. 106915, 2023.
[17] M. V. Anaraki and S. Farzin, "The Pine Cone Optimization Algorithm (PCOA)," Biomimetics, vol. 9, no. 2, p. 91, 2024.
[18] I. K. M. Jais and A. R. Ismail, "Adam Optimization Algorithm for Wide and Deep Neural Network," Knowledge Engineering and Data Science, vol. 2, no. 1, p. 41–46, 2019.
[19] F. Mehmood, S. Ahmad and T. K. Whangbo, "An Efficient Optimization Technique for Training Deep Neural Networks," Mathematics, vol. 11, no. 6, 2023.
[20] J. Wu, X.-Y. Chen, H. Zhang, L.-D. Xiong, H. Lei and S.-H. Deng, "Hyperparameter Optimization for Machine Learning Models Based on Bayesian Optimization," Journal of Electronic Science and Technology, vol. 17, no. 1, pp. 26-40, 2019.


## Authors' Profiles



**Choudari Lakshmi** is a research scholar at GITAM, Visakhapatnam. She also works as an Assistant Professor in the Department of Computer Science and Engineering at Gitam School of Technology. She has accumulated 8 years of teaching experience. Her areas of interest encompass Machine Learning, Deep Learning.



**Dr. Srinivasa Rao** obtained his doctoral degree in 2016, specializing in Image Processing. He is employed as an Associate Professor in the Department of Computer Science and Engineering at GITAM, Visakhapatnam. He has amassed 29 years of teaching experience. He is interested in researching Artificial Intelligence, Machine Learning and Soft Computing.

## How to cite this paper:

Choudari Lakshmi, Srinivasa Rao Konda, "Carbon Dioxide Emission Prediction for Trend Analysis using CAViaR Pine Cone Optimization Algorithm Enabled Attention-Based LSTM", International Journal of Information Technology and Computer Science(IJITCS), Vol.18, No.5, pp.138-150, 2026. DOI:10.5815/ijitcs.2026.05.09